

1. DEFORMATION OF UNLITHIFIED SEDIMENTS IN AN EARLY STAGE OF THE COMPACTION PROCESS DEDUCED FROM MICROTEXTURES AND MAGNETIC FABRICS: ODP LEG 174B, HOLE 1074A¹

Satoshi Hirano,² Yujiro Ogawa,³ and Kiichiro Kawamura⁴

ABSTRACT

To reveal compaction processes and mechanisms, we have studied microtextures and magnetic fabrics of unlithified sediments collected from Hole 1074A, on the eastern flank of the Mid-Atlantic Ridge, during Leg 174B. Samples consisted of nannofossil ooze with varying amounts of foraminifers, clay, radiolarians and sand. Scanning electron microscope observation shows that nannofossils and planktonic foraminifers in the sediments are well preserved, that void space in the unlithified sediments is formed by an assemblage of microfossils consisting of a staircase structure of nannofossils and an aggregation of foraminifers, and that the number of spine-shaped nannofossil fragments tends to increase with depth, suggesting weak deformation probably due to compaction occurring during burial. Anisotropy of magnetic susceptibility results, however, provide little obvious information about deformation of the sediments. These results are consistent with those of the onboard multisensor track measurements.

INTRODUCTION

The objective of this study is to reveal the deformation style of unlithified sediments in the early stage of compaction in a passive tectonic setting. Although extensive studies have been carried out on the

¹Hirano, S., Ogawa, Y., and Kawamura, K., 2001. Deformation of unlithified sediments in an early stage of the compaction process deduced from microtextures and magnetic fabrics: ODP Leg 174B, Hole 1074A. *In* Becker, K., and Malone, M.J. (Eds.), *Proc. ODP, Sci. Results*, 174B, 1–13 [Online]. Available from World Wide Web: <http://www-odp.tamu.edu/publications/174B_SR/VOLUME/CHAPTERS/SR174B01.PDF>. [Cited YYYY-MM-DD]

²Frontier Research Program for Subduction Dynamics, Japan Marine Science and Technology Center (JAMSTEC), Yokosuka, Kanagawa, 237-0061, Japan. hiranos@jamstec.go.jp

³Institute of Geoscience, University of Tsukuba, Tsukuba, Ibaraki, 305-8571, Japan.

⁴Fukada Geological Institute, Honkomagome, Bunkyo, Tokyo, 113-0021, Japan.

strain of accretionary prism sediments (e.g., Agar et al., 1989; Morgan and Karig, 1993; Hounslow, 1990; Owens, 1993; Housen and Sato, 1995), most studies lack comparisons between the fabrics measured in deformed prism sediments and those measured in undeformed sediments. Housen (1997) pointed out that an initial reference fabric is required to determine changes in fabric produced by tectonic deformation. One of the best ways to obtain an initial reference fabric is to look at sediments recovered from a passive tectonic setting or collected seaward of a deformation front.

In this paper, we report the results of scanning electron microscope (SEM) and magnetic fabric analyses of sediments recovered from Hole 1074A, on the eastern flank of the Mid-Atlantic Ridge, during Ocean Drilling Program (ODP) Leg 174B.

STUDY SITE

Hole 1074A is located at 22°46.8326'N, 46°6.7398'W, in an isolated sediment pond (North Pond) ~110 km east of the median valley of the Mid-Atlantic Ridge and 110 km south of the Kane Fracture Zone (Husson, et al., 1978; Becker, Malone, et al., 1998). North Pond is characterized by the low heat flow of a 7-Ma basement (Langseth et al., 1992). The location of Site 1074 is near the northwest edge of the pond, where a basement ridge emerges from the sediments and has a local high heat flow value.

At the single hole drilled at Hole 1074A (Shipboard Scientific Party, 1998), 64 m of sediments and 0.58 m of basalt were recovered. Two lithologic units were defined: Unit I, which contains nannofossil ooze with varying amounts of foraminifers, clay, radiolarians and sand, and nannofossil clay, overlying Unit II, which is a unit of aphyric basalt. The sedimentary Unit I was divided into two subunits based on the magnetic susceptibility record, clay content, and the presence or absence of graded sand layers. Subunit IA includes the upper 62 m of sediments; Subunit IB, a red clay, occupies the lower 2 m. The clay content gradually increases and the presence of sand (either foraminifer ooze or lithic fragments) decreases with depth in the hole.

Bulk X-ray diffraction (XRD) analysis indicates that the aluminosilicate mineral composition does not vary significantly between samples. Mineral phases identified by XRD include calcite, illite, chlorite, and plagioclase. Furthermore, data sets from Hole 395A, located at 4 km southeast from Site 1174A in the same isolated sedimentary pond, are useful as a reference. With few exceptions, the most abundant component of the clay mineral complex is mixed-layer mineral of the montmorillonite-hydromica (M-H) type with a strong smectite component. The next most abundant clays are usually, in descending order, hydromica (illite), chlorite, kaolinite, palygorskite, and, less frequently, a mixed-layer mineral of the second type of the mica-montmorillonite composition (H-M) (Timofeev et al., 1978).

The magnetic susceptibility values, deduced from the onboard multi-sensor track (MST), increase in intervals with increasing clay content, bioturbation, and sand layers. Foraminifer oozes are characterized by very low susceptibility values. The magnetic susceptibility values are generally low in the upper 45 meters below seafloor (mbsf), increase sharply at the Subunit IA/IB contact, and remain high in Subunit IB.

Acoustic velocity increases from seawater values at the seafloor to >1500 m/s at 12 mbsf. Below this depth, velocity does not increase with

depth, but higher velocity intervals (~1600 m/s) occur throughout and are associated with coarser-grained intervals. When compared with the susceptibility record, high-velocity values correspond to coarse-grained intervals, whereas susceptibility corresponds only to nonforaminifer coarse-grained intervals.

METHODOLOGY AND TERMINOLOGY

During the cruise, individual oriented samples were taken in relatively undisturbed working halves of the cores. A total of 112 samples were taken at ~50- to 80-cm intervals from Unit I (Shipboard Scientific Party, 1998). We collected each sample by pushing a standard ODP sample box (6.06 cm³) until the box was full. We then inserted a sharp knife to cut off and to support the sample during removal. All samples were immediately sealed in plastic bags with wet sponges to protect against drying.

On shore, we measured the anisotropy of magnetic susceptibility (AMS) of each sample with a Kappabridge KLY-3S magnetic susceptibility meter (Table T1). After completing magnetic fabric measurements, we proceeded to SEM observation using the same samples.

Before SEM observation, we fixed wet and fragile samples using a freeze-drying method (e.g., O'Brien, 1970; Gillott, 1975). In this study, we used the t-butyl alcohol freeze-drying method described as follows (Takizawa et al., 1995): After all samples were placed in ethanol, they were dipped into t-butyl alcohol, frozen using liquid nitrogen, and dried in a vacuum evaporator. We selected about 30 specimens for SEM observation. These SEM specimens were investigated by a scanning electron microscope operating at 5 kV. The rest were preserved in a t-butyl bath for future analysis. The reliability of the above procedure was proven in a previous study by Takizawa and Ogawa (1999), who have succeeded in describing microstructure in the scaly fabric portion from the basal décollement zone of the northern Barbados accretionary prism.

To estimate the relative abundance of broken coccolith fragments in a specimen, we basically followed the visual estimation technique (Mazzullo et al., 1988) on a SEM photo by using a standard visual comparison chart. The relative number of fragments were classified into six categories: dominant (>50%–100%), abundant (>20%–50%), common (>5%–20%), present (>1%–5%), rare (>0.1%–1%), and trace (0%–0.1%) in descending order.

To describe a magnetic anisotropy, a Flinn-type diagram has been conventionally used to plot a measure of foliation against that of lineation as this is analogous to the plots of strain or shape ratios commonly used in structural geology (Flinn, 1962, 1965). The eccentricity of the anisotropy ellipsoid can be expressed mainly in terms of the ratios of the axial values. These parameters, i.e., lineation, L , and foliation, F , are given by

$$L = K_{\max}/K_{\text{int}} \text{ (Balsley and Buddington, 1960) and}$$

$$F = K_{\text{int}}/K_{\min} \text{ (Stacey et al., 1960),}$$

where K_{\max} , K_{int} , and K_{\min} are the maximum, intermediate, and minimum axes of the susceptibility ellipsoid, respectively. On this diagram, oblate

T1. AMS results, Hole 1074A,
p. 12.

fabrics plot below the slope of unit gradient and prolate fabrics plot above.

RESULTS

Microtextures

Unbroken nannofossils are preserved throughout the sampled section (Fig. F1). Although the number of spine-shaped fragments of nannofossil is small (less than 5% at most), it tends to increase with depth. At 19.45 mbsf (Sample 174B-1074A-3H-1, 45–47 cm) (Fig. F1A), the relative abundance is trace (0%–0.1%), whereas it is present (>1%–5%) at 60.05 mbsf (Sample 174B-1074A-7H-3, 5–7 cm) (Fig. F1D).

The arrangement of nannofossils plays an important role in creating a void space in the unlithified sediments. Coccoliths are linked edge to edge and edge to face in all samples. In the case of clay minerals, such as kaolinite, such a fabric results in an open framework with very high porosity (Bennett and Hulbert, 1986). Even at 60.80 mbsf (Sample 174B-1074A-7H-3, 5.0–7.0 cm), both the edge-to-face and edge-to-edge linked coccoliths were preserved (Fig. F1D). This indicates that the void space is still maintained until this depth because the deformation of the sediments is weak.

Shape and volume of the void space are controlled by type of aggregation pattern and material features. In a nannofossil dominated sample, the edge-to-face or edge-to-edge linked coccoliths make a stairstep structure (O'Brien, 1971). Such void space is generally of random shape, with sizes ranging from a few to several tens of micrometers. On the other hand, a sample that contains well-preserved planktonic foraminifers (e.g., 174B-1074A-5H-4, 40–42 cm; 38.40 mbsf) (Fig. F1C) has a large void space (~100 μm in diameter) and seems to be less consolidated in that the foraminifers are few or absent. In addition, some stairstep structures of nannofossil aggregation develop in a larger void space and are surrounded by foraminifers. This structure might play the role of beam, supporting the wall of the larger void space from inside.

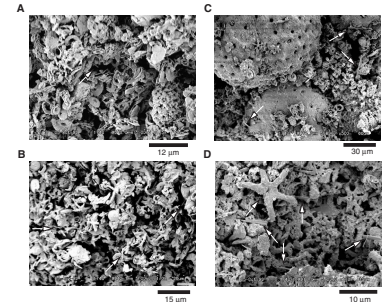
The SEM observation shows that nannofossils and planktonic foraminifers in the sediments are well preserved and that void space in the unlithified sediments is formed by an assemblage of microfossils consisting of a stairstep structure of nannofossils and aggregation of foraminifers.

Magnetic Fabrics

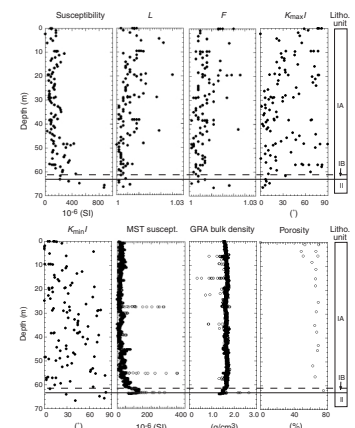
Using AMS measurements, we could not detect any obvious deformation of the unlithified sediments. The vertical change of magnetic susceptibility measured on shore using discrete samples is consistent with that obtained by the MST measurements during the cruise. The magnetic susceptibility, which varies from $\sim 30 \times 10^{-6}$ SI to $\sim 880 \times 10^{-6}$ SI, tends to increase with depth and is sensitive to lithologic variations (Fig. F2). Particularly, the magnetic susceptibility is high in Subunit IB, which contains many small (<1 cm) basalt clasts.

The L and F values, which represent lineation and foliation of magnetic fabrics, are variable but tend to be weaker with depth. Both the L and F values decrease from 1.02 near the seafloor to <1.005 at the base of Unit I (63.5 mbsf). These results indicate that anisotropy of magnetic fabrics tends to be weaker with depth regardless of initial configuration.

F1. Microtextures of unlithified sediments, p. 9.



F2. Downhole profiles, p. 10.



The Flinn diagram of L vs. F shows that most plots are scattered around the left bottom of the diagram, ranging from ~ 1 to 1.025, along the slope of unit gradient (Fig. F3). This also indicates that the anisotropy is weak or almost neutral.

DISCUSSION

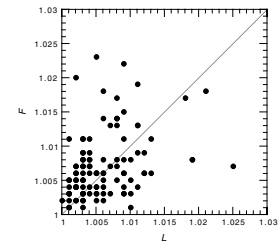
The SEM observation shows that nannofossils and planktonic foraminifers in the sediments are well preserved throughout. Particularly, assemblage of nannofossils plays an important role in making a void space in the unlithified sediments. Although the number of spine-shaped fragments of nannofossils is small, it tends to increase with depth (Fig. F1). These occurrences suggest that weak deformation, probably due to compaction, occurred during burial. The shape and volume of the void space are controlled by the type of aggregation pattern and material features. In the case of clay minerals, such as kaolinite, this type of fabric results in an open internal floccule framework with very high porosity, (Bennett and Hulbert, 1986) possibly more than 80%. By using AMS measurements, on the other hand, we could not detect any anisotropy of the unlithified sediments. The Flinn diagram of L vs. F shows that the anisotropy is almost neutral (Fig. F3). This is consistent with the SEM observation results. The increase of the magnetic susceptibility with depth can be explained by successive compaction processes of the sediments and an increasing number of basalt clasts. The unit volume of sediment reduced during burial so that the numbers of magnetic fabrics in each unit volume increase with depth.

The results of previous experimental investigation of the behavior of clay soils during loading are relevant to the type of deformation and all rocks that contain clay materials. Although oriented fabrics can be formed in kaolinite and montmorillonite pastes, the strongest orientations occur mainly in illite-bearing pastes (e.g., Tarling and Hrouda, 1933). In addition, simple shear tends to strengthen montmorillonite clay structures but to destroy the cohesion of kaolinite clays. However, the initial fabrics are determined by gravitational and hydrodynamic forces, such as bottom current, and are controlled mainly by the size, shape, and mass of the detrital grains in a passive environment. On the other hand, if the sediments experienced a strong simple shear deformation (e.g., sediments just above the décollement zone at the Nankai accretionary prism or at the Barbados accretionary prism), the anisotropy of magnetic susceptibility of these sediments tends to be larger (e.g., Owens, 1993; Housen, 1997). The sediments in Hole 1074A contain kaolinite, montmorillonite, and illite and represent little anisotropy. This might be due to only vertical loading, although quantitative investigation will be required in the future.

The onboard gamma-ray attenuation bulk densiometer (GRA bulk density) measurement and porosity data show no significant change in either the density or porosity throughout (Fig. F2). The GRA bulk density is almost constant, varying from 1.5 to 1.7 g/cm³. Porosity of discrete samples varies from 60% to 70% throughout, except when above 10 mbsf, where porosity ranges from 40% to 70%.

The data sets in this study should be quantified for future application to active tectonic settings as a reference of the initial condition and for comparison with various tectonic settings. In fact, the behavior of unlithified sediments (i.e., consolidation processes) varies in each accretionary prism because the contents of sediments are different in each

F3. Flinn diagram of L vs. F of sediments, p. 11.



area. For example, large-sized grain (e.g., foraminifer) content might exert control on the degree of sediment consolidation. Such large-sized grain content could be quantified by counting foraminifers under the SEM or on smear slides or by weight percent through grain size separations. Compaction of sediments could be quantified through porosity measurements, although the initial porosity of a given sample will never be known. The process of compaction could be studied through consolidation tests, allowing the compaction process of various unlithified sediments to be clarified quantitatively.

SUMMARY

In order to clarify processes of an early stage of compaction of unlithified sediments, we conducted SEM observation of microtexture and magnetic fabric analyses of nannofossil ooze, which was collected from Hole 1074A, on the eastern flank of the Mid-Atlantic Ridge, during ODP Leg 174B. We are able to make the following observations:

1. SEM observation shows that nannofossils and planktonic foraminifers in the sediments are well preserved and that void space in the unlithified sediments is formed by an assemblage of microfossils consisting of a stairstep structure of nannofossils and aggregation of foraminifers.
2. Although the number of spine-shaped fragments of nannofossils is small (<5% at most), it tends to increase with depth. This is probably due to weak compaction by self-loading.
3. AMS results, however, provide little obvious information about deformation of the sediments. These results are consistent with those of onboard MST measurements.

ACKNOWLEDGMENTS

We would like to express our gratitude to Ken Ikehara for permitting us to use the magnetic fabric measurement system at the Geological Survey of Japan. We also thank Takami Kawada for assistance in the SEM observation at the University of Tsukuba. We also acknowledge Toshiya Kanamatsu, Japan Marine Science and Technology Center, for fruitful discussions.

REFERENCES

- Agar, S.M., Prior, D.J., and Behrmann, J.H., 1989. Back-scattered electron imagery of the tectonic fabrics of some fine-grained sediments: implications for fabric nomenclature and deformation processes. *Geology*, 17:901–904.
- Balsley, J.R., and Buddington, A.F., 1960. Magnetic susceptibility anisotropy and fabric of some Adirondack granites and orthogneisses. *Am. J. Sci.*, 2:6–20.
- Becker, K., Malone, M.J., et al., 1998. *Proc. ODP, Init. Repts.*, 174B: College Station, TX (Ocean Drilling Program).
- Bennett, R.H., and Hulbert, M.H., 1986. *Clay Microstructure*: Boston (International Human Resources Development Corp. Publ.).
- Flinn, D., 1962. On folding during three-dimensional progressive deformation. *Q. J. Geol. Soc. London*, 105:711.
- Flinn, D., 1965. On the symmetry principle and the deformation ellipsoid. *Geol. Mag.*, 102:36–45.
- Gillott, J.E., 1975. Importance of specimen preparation in microscopy. In *Soil Specimen Preparation for Laboratory Testing*. ASTM Tech. Publ., 599:289–307.
- Hounslow, M.W., 1990. Grain fabric measured using magnetic susceptibility anisotropy in deformed sediments of the Barbados Accretionary Prism: Leg 110. In Moore, J.C., Mascle, A., et al., *Proc. ODP, Sci. Results*, 110: College Station, TX (Ocean Drilling Program), 257–275.
- Housen, B.A., 1997. Magnetic anisotropy of Barbados prism sediments. In Shipley, T.H., Ogawa, Y., Blum, P., and Bahr, J.M. (Eds.), *Proc. ODP, Sci. Results*, 156: College Station, TX (Ocean Drilling Program), 97–105.
- Housen, B.A., and Sato, T., 1995. Magnetic anisotropy fabrics from the Cascadia accretionary prism. In Carson, B., Westbrook, G.K., Musgrave, R.J., and Suess, E. (Eds.), *Proc. ODP, Sci. Results*, 146 (Pt 1): College Station, TX (Ocean Drilling Program), 233–254.
- Hussong, D.M., Fryer, P.B., Tuthill, J.D., and Wippernan, L.K., 1978. The geological and geophysical setting near DSDP Site 395, North Atlantic Ocean. In Melson, W.G., Rabinowitz, P.D., et al., *Init. Repts. DSDP*, 45: Washington (U.S. Govt. Printing Office), 23–38.
- Langseth, M.G., Becker, K., Von Herzen, R.P., and Schultheiss, P., 1992. Heat and fluid flux through the sediment on the western flank of the Mid-Atlantic Ridge: a hydrological study of North Pond. *Geophys. Res. Lett.*, 19:517–520.
- Mazzullo, J., and Graham, A.G. (Eds.), 1988. *Handbook for Shipboard Sedimentologists*. ODP Tech. Note, 8.
- Morgan, J.K., and Karig, D.E., 1993. Ductile strains in clay-rich sediments from Hole 808C: preliminary results using X-ray pole figure goniometry. In Hill, I.A., Taira, A., Firth, J.V., et al., *Proc. ODP, Sci. Results*, 131: College Station, TX (Ocean Drilling Program), 141–155.
- O'Brien, N.R., 1970. Freeze drying technique in the study of the fabric of moist clay sediment. *J. Electron Microsc.*, 19:277.
- O'Brien, N.R., 1971. Fabric of kaolinite and illite floccules. *Clays Clay Miner.*, 19:353–359.
- Owens, W.H., 1993. Magnetic fabric studies of samples from Hole 808C, Nankai Trough. In Hill, I.A., Taira, A., Firth, J.V., et al., *Proc. ODP, Sci. Results*, 131: College Station, TX (Ocean Drilling Program), 301–310.
- Shipboard Scientific Party, 1998. Site 1074. In Becker, K., Malone, M.J., et al., *Proc. ODP, Init. Repts.*, 174B: College Station, TX (Ocean Drilling Program), 25–35.
- Stacey, F.D., Joplin, G., and Lindsay, J., 1960. Magnetic anisotropy and fabric of some foliated rocks from S.E. Australia. *Geofis. Pura Appl.*, 47:30–40.
- Takizawa, S., Kawata, T., and Ohono, Y., 1995. A method of fixation and freeze drying of soft sediments containing water. *Chishitsugaku Zasshi [J. Geol. Soc. Jpn.]*, 101:941–944.

- Takizawa, S., and Ogawa, Y., 1999. Dilatant clayey microstructure in the Barbados decollement zone. *J. Struct. Geol.*, 21:117–122.
- Tarling, D.H., and Hrouda, F., 1993. *The Magnetic Anisotropy of Rocks*: London (Chapman and Hall).
- Timofeev, P.P., Varentsov, I.M., Rateev, M.A., and Renngarten, N.V., 1979. Lithology, mineralogy, and geochemistry of upper Cenozoic sediments at 23°N near the Mid-Atlantic Ridge, drilled on Leg 45. *In* Melson, W.G., Rabinowitz, P.D., et al., *Init. Repts. DSDP*, 45: Washington (U.S. Govt. Printing Office), 323–347.

Figure F1. Microtextures of unlithified sediments. Note that the number of broken fragments (white arrows) increases with depth, from A to D. **A.** Well-preserved coccoliths link edge-to-face (a stairstep structure), forming a large amount of void space (Sample 174B-1074A-3H-1, 45–47 cm; 19.45 mbsf). The relative abundance of coccolith fragments is trace (0%–0.1%). **B.** A stairstep structure is still maintained in this depth (Sample 174B-1074A-4H-1, 45–47 cm; 28.95 mbsf). The relative abundance of coccolith fragments is rare (>0.1%–1%). **C.** Well-preserved planktonic foraminifers aggregate and contact each other, resulting in a large void surrounded by each foraminifer's surface. (Sample 174B-1074A-5H-4, 40–42 cm; 42.90 mbsf). The relative abundance of coccolith fragments is present (>1%–5%). **D.** Both the edge-to-face and edge-to-edge linked coccoliths were preserved until this depth (Sample 174B-1074A-7H-3, 5–7 cm; 60.05 mbsf). The relative abundance of coccolith fragments is present (>1–5%).

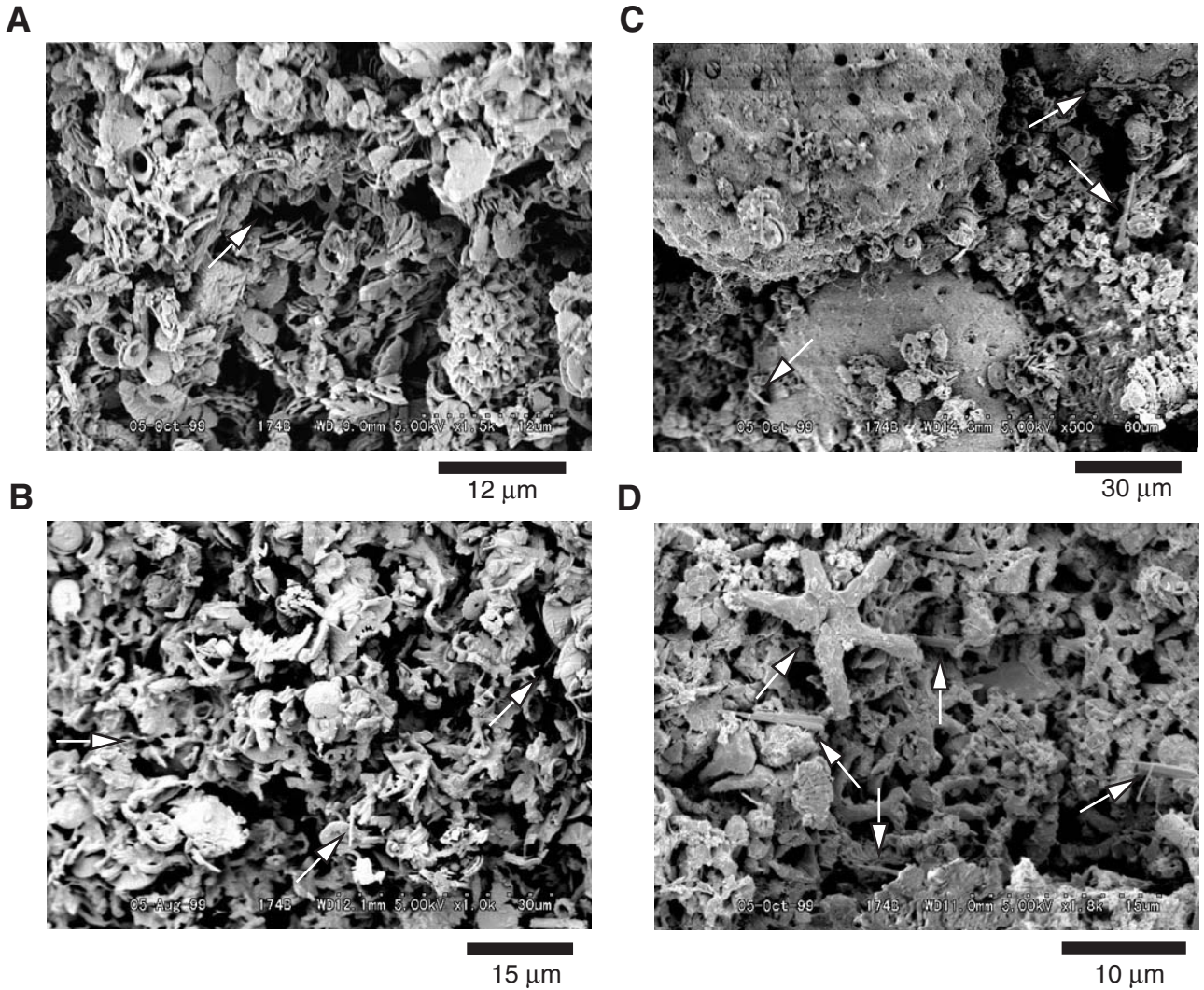


Figure F2. Downhole profiles of magnetic susceptibility, L (magnetic lineation), F (magnetic foliation), K_{\max} and K_{\min} inclinations, MST magnetic susceptibility, GRA bulk density, porosity, and lithologic units.

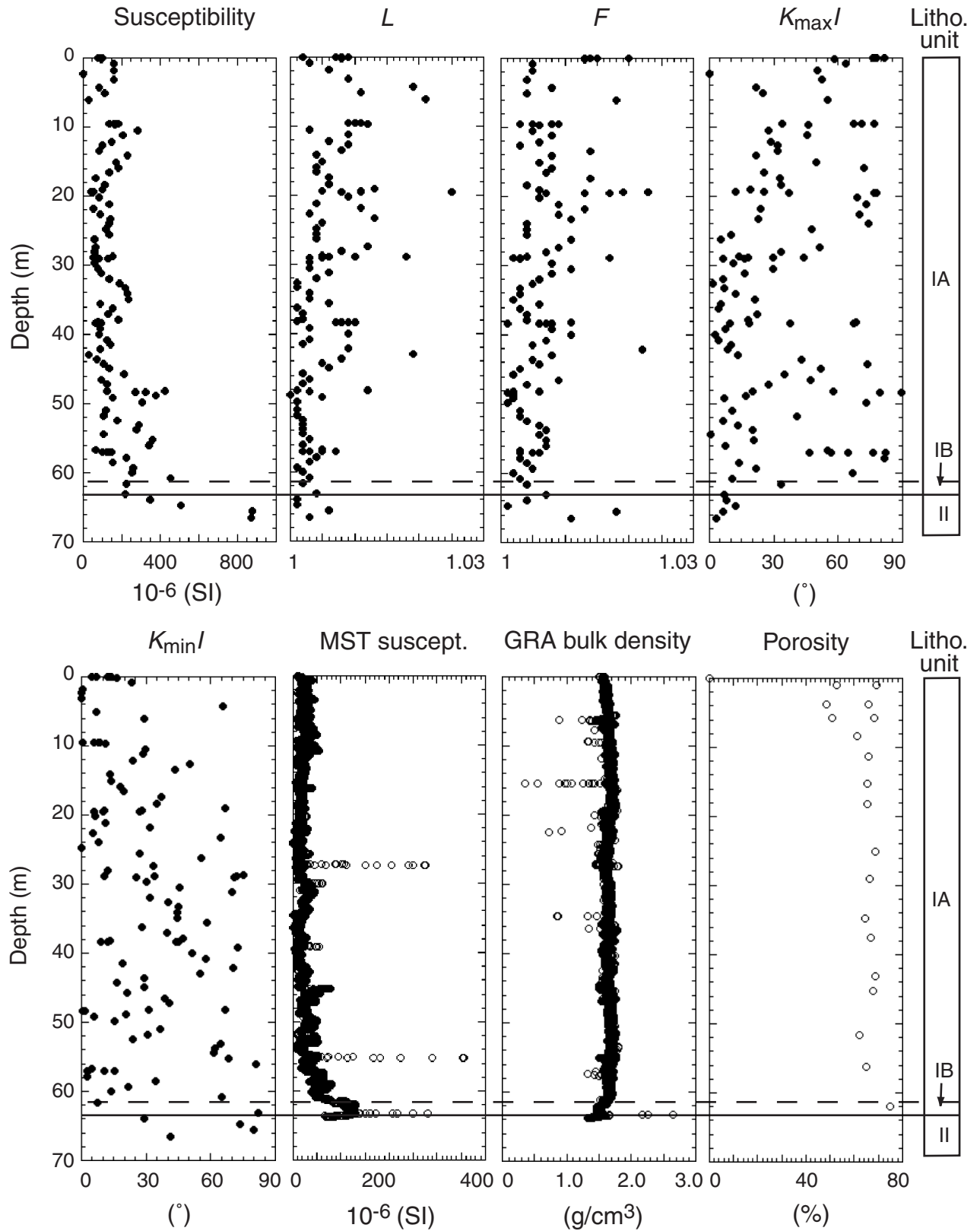


Figure F3. Flinn diagram of L vs. F of sediments from Hole 1074A. L and F correspond to K_{\max}/K_{int} (lineation) and $K_{\text{int}}/K_{\text{min}}$ (foliation), respectively.

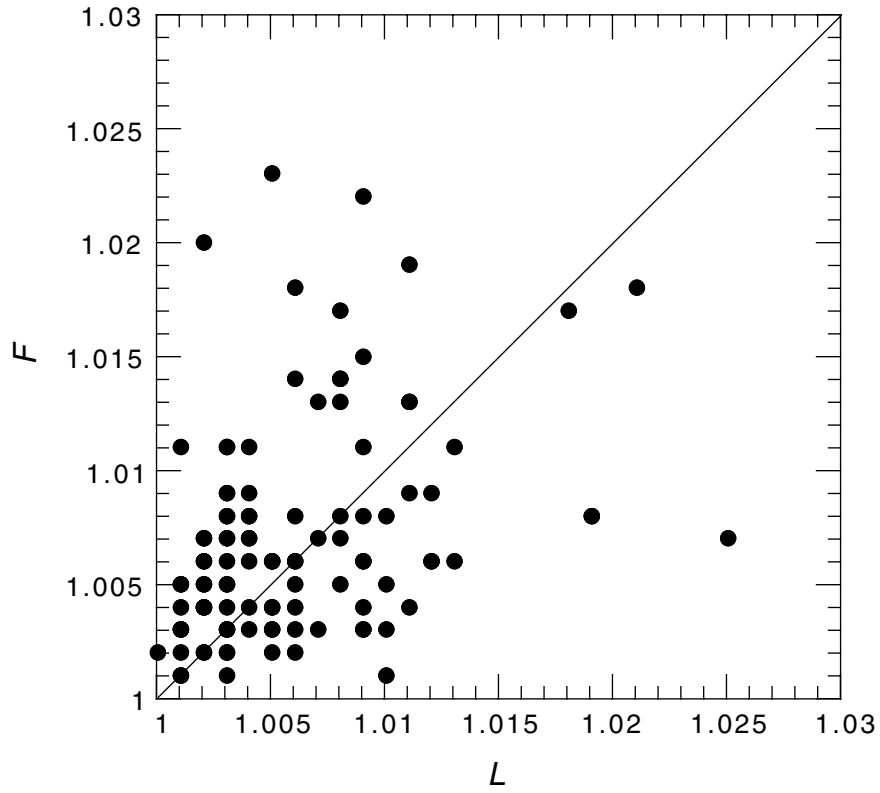


Table T1. AMS results at Hole 1074A obtained from discrete samples. L , F , $K_{max}I$, and $K_{min}I$ correspond to magnetic lineation, magnetic foliation, inclination of maximum axis of susceptibility ellipsoid, and inclination of minimum axis susceptibility ellipsoid, respectively.

Core, section, interval (cm)	Depth (mbsf)	Susceptibility (10^{-6})	L	F	$K_{max}I$	$K_{min}I$
174B-1074A-						
1H-1, 0.0-2.0	0.00	96.1	1.007	1.013	76.2	13.7
1H-1, 2.5-4.5	0.03	79.5	1.002	1.020	81.8	6.9
1H-1, 5.0-7.5	0.05	95.7	1.009	1.015	77.5	4.6
1H-1, 7.5-9.5	0.08	99.9	1.008	1.014	77.9	12.1
1H-1, 10.0-12.0	0.10	96.1	1.008	1.013	58.2	16.5
1H-1, 80.0-82.0	0.80	160.0	1.003	1.005	63.5	23.2
1H-2, 30.0-32.0	1.80	157.0	1.006	1.005	50.4	0.5
1H-2, 80.0-82.0	2.30	—	—	—	—	—
1H-3, 20.0-22.0	3.20	157.0	1.009	1.004	52.5	0.2
1H-3, 128.0-130.0	4.28	83.5	1.019	1.008	21.5	65.5
1H-4, 65.0-67.0	5.15	112.0	1.011	1.004	24.8	6.8
1H-5, 15.0-17.0	6.15	31.9	1.021	1.018	54.9	29.0
2H-1, 0.5-2.5	9.51	138.0	1.010	1.005	67.2	8.7
2H-1, 2.5-4.5	9.53	159.0	1.009	1.003	33.7	0.7
2H-1, 5.5-7.5	9.56	177.0	1.011	1.009	76.9	8.0
2H-1, 8.0-10.0	9.58	183.0	1.010	1.008	70.8	5.7
2H-1, 10.0-12.5	9.61	165.0	1.012	1.006	46.0	11.0
2H-1, 105.0-107.0	10.55	283.0	1.003	1.005	27.3	29.8
2H-2, 9.5-11.5	11.10	206.0	1.009	1.008	45.5	28.8
2H-2, 110.0-112.0	12.10	149.0	1.006	1.006	28.5	24.1
2H-3, 6.0-8.0	12.56	99.0	1.009	1.003	31.7	50.4
2H-3, 90.0-92.0	13.40	80.6	1.008	1.014	31.7	43.6
2H-4, 6.0-8.0	14.06	229.0	1.004	1.008	21.8	13.0
2H-4, 110.0-112.0	15.10	171.0	1.005	1.006	49.9	13.8
2H-5, 35.0-37.0	15.85	183.0	1.004	1.008	72.0	18.0
2H-5, 110.0-112.0	16.60	137.0	1.004	1.007	25.2	19.7
2H-6, 46.0-48.0	17.46	65.9	1.006	1.014	32.8	37.0
2H-6, 130.5-132.5	18.31	112.0	1.006	1.004	33.3	35.2
2H-7, 60.0-62.0	19.10	97.6	1.013	1.006	18.9	66.5
3H-1, 35.0-37.0	19.35	44.1	1.011	1.019	25.2	27.9
3H-1, 40.0-42.0	19.40	52.7	1.005	1.023	12.2	10.5
3H-1, 45.0-47.0	19.45	47.9	1.011	1.013	76.9	6.0
3H-1, 50.0-52.0	19.50	45.9	1.025	1.007	37.1	27.2
3H-1, 55.0-57.0	19.55	49.1	1.008	1.017	78.1	10.1
3H-1, 120.0-122.0	20.20	80.6	1.009	1.006	68.8	6.6
3H-2, 60.0-62.0	21.10	137.0	1.004	1.009	73.3	11.2
3H-2, 130.0-132.0	21.80	53.1	1.011	1.013	24.1	32.0
3H-3, 60.0-62.0	22.60	86.7	1.003	1.009	69.9	5.2
3H-3, 125.0-127.0	23.25	141.0	1.013	1.011	22.9	64.7
3H-4, 40.0-42.0	23.90	135.0	1.005	1.004	74.0	7.9
3H-4, 130.0-132.0	24.80	118.0	1.004	1.004	47.9	0.1
3H-5, 55.5-57.5	25.56	133.0	1.004	1.004	10.2	27.0
3H-5, 130.5-132.5	26.31	59.1	1.004	1.011	5.4	55.5
3H-6, 90.5-92.5	27.41	64.8	1.012	1.009	51.5	33.2
3H-7, 5.0-7.0	28.05	59.9	1.008	1.007	33.4	12.3
3H-7, 70.0-72.0	28.70	151.0	1.005	1.004	13.8	75.3
4H-1, 30.0-32.0	28.80	53.1	1.006	1.002	43.9	33.8
4H-1, 35.0-37.0	28.85	69.0	1.010	1.003	29.5	10.6
4H-1, 40.0-42.0	28.39	58.9	1.018	1.017	17.9	72.1
4H-1, 45.0-47.0	28.95	82.6	1.005	1.003	16.5	71.1
4H-1, 50.0-52.0	29.00	127.0	1.003	1.003	6.5	25.7
4H-1, 125.0-127.0	29.75	59.0	1.003	1.008	11.4	30.1
4H-2, 50.0-52.0	30.50	75.2	1.003	1.011	29.5	45.8
4H-2, 120.0-122.0	31.20	97.0	1.006	1.008	16.4	69.9
4H-3, 40.0-42.0	31.90	134.0	1.004	1.006	6.3	31.9
4H-3, 110.0-112.0	32.60	189.0	1.001	1.005	1.7	40.2
4H-4, 34.5-36.5	33.35	217.0	1.001	1.003	7.1	45.1
4H-4, 115.0-117.0	34.15	231.0	1.003	1.003	12.1	44.7
4H-5, 35.0-37.0	34.85	234.0	1.003	1.002	21.3	44.5
4H-5, 115.0-117.0	35.65	91.5	1.006	1.006	5.1	58.0
4H-6, 30.0-32.0	36.30	154.0	1.001	1.003	4.4	27.9
4H-6, 105.0-107.0	37.05	129.0	1.002	1.004	22.2	39.5
4H-7, 35.0-37.0	37.85	182.0	1.002	1.004	18.2	47.4

Table T1 (continued).

Core, section, interval (cm)	Depth (mbsf)	Susceptibility (10 ⁻⁶)	<i>L</i>	<i>F</i>	<i>K</i> _{max} / <i>I</i>	<i>K</i> _{min} / <i>I</i>
5H-1, 24.5-26.5	38.25	79.5	1.001	1.011	68.3	13.2
5H-1, 29.5-31.5	38.30	96.3	1.010	1.001	67.5	8.8
5H-1, 35.0-37.0	38.35	85.6	1.007	1.007	9.7	12.1
5H-1, 40.0-42.0	38.40	87.7	1.009	1.006	18.7	45.2
5H-1, 45.0-47.0	38.45	64.4	1.008	1.008	37.6	44.1
5H-1, 115.0-117.0	39.15	86.0	1.003	1.008	7.5	72.5
5H-2, 55.0-57.0	40.05	84.4	1.009	1.011	2.8	51.3
5H-2, 125.0-127.0	40.75	125.0	1.003	1.007	4.5	57.8
5H-3, 50.0-52.0	41.50	143.0	1.002	1.005	9.9	19.1
5H-3, 120.0-122.0	42.20	88.2	1.009	1.022	8.4	70.6
5H-4, 40.0-42.0	42.90	31.2	1.019	1.008	13.1	55.2
5H-4, 110.0-112.0	43.60	73.4	1.008	1.005	42.9	29.0
5H-5, 23.0-25.0	44.23	107.0	1.005	1.006	73.7	16.2
5H-5, 100.0-102.0	45.00	138.0	1.006	1.003	51.8	29.3
5H-6, 30.5-32.5	45.81	212.0	1.002	1.002	35.2	21.3
5H-6, 102.5-104.5	46.53	94.1	1.003	1.009	47.0	38.8
5H-7, 20.0-22.0	47.20	125.0	1.002	1.004	27.6	41.0
6H-1, 64.5-66.5	48.15	122.0	1.012	1.006	20.3	66.8
6H-1, 74.5-76.5	48.25	425.0	1.001	1.002	57.7	31.4
6H-1, 87.0-89.0	48.37	272.0	1.003	1.002	89.3	0.7
6H-1, 92.0-94.0	48.42	326.0	1.003	1.001	79.3	1.5
6H-1, 135.0-137.0	48.85	375.0	1.000	1.002	17.1	20.9
6H-2, 25.0-27.0	49.25	154.0	1.005	1.002	7.1	5.9
6H-2, 90.0-92.0	49.90	305.0	1.001	1.001	73.2	15.5
6H-3, 55.0-57.0	51.05	116.0	1.001	1.003	10.8	36.5
6H-3, 125.0-127.0	51.75	105.0	1.001	1.003	40.9	30.8
6H-4, 45.0-47.0	52.45	175.0	1.002	1.004	6.2	23.6
6H-4, 115.0-117.0	53.15	287.0	1.002	1.006	13.5	64.6
6H-5, 35.0-37.0	53.85	274.0	1.002	1.007	20.3	62.1
6H-5, 100.5-102.5	54.51	106.0	1.002	1.006	0.3	61.5
6H-6, 30.5-32.5	55.31	362.0	1.003	1.007	20.9	68.5
6H-6, 100.5-102.5	56.01	341.0	1.002	1.007	7.5	80.8
6H-7, 20.5-22.5	56.71	65.5	1.005	1.003	55.0	4.7
7H-1, 0.0-2.0	57.00	131.0	1.007	1.003	56.6	15.2
7H-1, 2.5-4.5	57.03	147.0	1.007	1.003	46.7	2.5
7H-1, 5.0-7.0	57.05	142.0	1.005	1.006	76.5	10.4
7H-1, 7.5-9.5	57.08	125.0	1.003	1.006	64.6	10.4
7H-1, 10.0-12.0	57.10	99.5	1.002	1.005	82.0	3.0
7H-1, 80.0-82.0	57.80	223.0	1.004	1.003	81.7	2.9
7H-2, 10.0-12.0	58.60	156.0	1.003	1.004	13.8	34.4
7H-2, 80.0-82.0	59.30	258.0	1.001	1.005	21.5	21.8
7H-3, 5.0-7.0	60.05	254.0	1.002	1.002	66.6	13.7
7H-3, 80.0-82.0	60.80	452.0	1.003	1.003	10.8	65.4
7H-4, 10.0-12.0	61.60	226.0	1.002	1.004	33.2	7.4
7H-5, 16.0-18.0	63.16	220.0	1.004	1.007	6.9	82.1
7H-5, 90.0-92.0	63.90	348.0	1.001	1.004	7.8	29.3
7H-6, 30.0-32.0	64.80	507.0	1.001	1.001	12.1	73.7
7H-6, 110.0-112.0	65.60	879.0	1.006	1.018	6.5	80.1
7H-7, 50.0-52.0	66.50	873.0	1.003	1.011	3.1	41.3

Notes: *L* = lineation, *F* = foliation. Dashes are data that was measured but not recorded because of operation error or other problems.